Article ID: 1000-7032(2024)01-0157-12

Exosome-triggered Metal Halide Perovskite-mediated Strategy of Circulating Tumors Cells Detection for Melanoma

CHEN Zhishan†, XU Pengfei†, ZHANG Shaoan, LI Yang*

(*School of Biomedical Engineering, Guangzhou Medical University, Guangzhou* 511436, *China*)

* *Corresponding Author, E-mail: lychris@sina.com*

Abstract: The emerging technique of liquid biopsy opens up a new opportunity for the rapid and accurate diagnosis of melanoma tumor featuring high metastatic tendency and mortality rates. However, the accuracy and sensitivity for liquid biopsy of melanoma are still limited, due to the use of low-expression epithelial cell adhesion molecule (EpCAM) to achieve enrichment of circulating tumor cells (CTCs) and subaltern photoluminescence quantum yields (PLQYs) organic probes as signal indicators. Here, we construct a new strategy of CTCs detection for liquid biopsy of melanoma by employing high-PLQYs metal halide perovskite (MHP) quantum dots and melanoma-derived exosome (MEX) as signal indicators and recognition analytes, respectively. The synthesized composites (PSPE) exhibit the superiorities on perfect hydrophilicity and hypotoxicity. In contrast to commercial EpCAM-triggered products, the detection sensitivity of our reagent materials is raised up by an order of magnitude. All results predict the potential of exosome-triggered MHP-mediated CTCs detection in accurate melanoma diagnosis of liquid biopsy.

Key words: melanoma; exosome; circulating tumor cells; metal halide perovskite; liquid biopsy

CLC number: O482.31 **Document code**: A **DOI**: 10.37188/CJL.20230237

黑色素瘤循环肿瘤细胞检测的金属卤化物钙钛矿外泌体复合探针检测新策略

陈志山†, 徐朋飞†, 张绍安, 李 杨*

(广州医科大学 生物医学工程学院, 广东 广州 511436)

摘要: 液体活检技术的兴起为黑色素瘤的快速、准确诊断提供了新的机遇。然而,普通循环肿瘤细胞活检基于上皮黏附蛋白进行阳性富集,但信号标记的有机荧光探针存在量子效率低的问题,导致检测黑色素瘤循环肿瘤细胞时准确率和灵敏度较低。本文以高量子效率的金属卤化物钙钛矿量子点作为信号标记物,以黑色素瘤来源的外泌体作为生物识别分子,构建了一种用于黑色素瘤液体活检的循环肿瘤细胞检测新策略。与商品化的上皮细胞黏附蛋白富集策略相比,本研究报道的复合探针检测新策略,其检测灵敏度提高了一个数量级,并且具有良好的亲水性和低毒性。实验结果证明了外泌体引导的金属卤化物钙钛矿量子点指示的黑色素瘤循环肿瘤细胞检测新策略具有理想的应用前景。

关 键 词: 黑色素瘤; 外泌体; 循环肿瘤细胞; 金属卤化物钙钛矿; 液体活检

收稿日期: 2023-10-12; **修订日期**: 2023-11-01

基金项目: 国家自然科学基金(52172083); 广东省国际科技合作计划(2021A0505030078); 广州市重点研发计划(2023B03J1239); 广州市教育系统创新学术团队计划(202235404); 中国博士后科学基金(2022M720919)

Supported by National Natural Science Foundation of China (52172083); International Science & Technology Cooperation Program of Guangdong (2021A0505030078); Guangzhou Key Research and Development Program (2023B03J1239); Program for Innovative Research Team in University of Education System of Guangzhou (202235404); China Postdoctoral Science Foundation (2022M720919)

†: 共同贡献作者

1 Introduction

Melanoma derived from epidermal improperly proliferating melanocytes is featured by a high metastatic tendency and high mortality rates, and now become a highly malignant tumor[1-2]. Conventional melanoma diagnosis starts from abnormalities of biochemical indicators. Recently, the use of liquid biopsy has provided new opportunities to rapidly identify melanoma tumor progression, since liquid biopsy can complement tumor biopsy to effectively obtain pathological information by enabling contributing biomarkers[3-4]. Circulating tumor cells (CTCs) released by the primary tumor or metastasis become one of the popular biomarkers, and are extensively investigated in liquid biopsy, due to the large heterogeneity deriving from the transport from the primary location to other, distant and susceptible tissues, as well as the formation of micro- and/or macro-metastases[5-6]. However, in clinical diagnosis, the development of CTCs detection for liquid biopsy of melanoma is still limited, as the lack of accuracy and sensitivity[7-9].

Actually, for accurate and sensitive CTCs detection of melanoma in liquid biopsy, the alternative strategy should possess standard targeted recognition capability and sensitively positive fluorescence feedback[10-11]. whereas, the existing route just depends on the epithelial cell adhesion molecule(EpCAM) to achieve CTCs enrichment, and employs organic probes as signal indicators to feedback results[12-13]. EpCAM is a transmembrane glycoprotein that has received more attention as a "universal" targeted molecule of tumors for the increase of cell concentration in sample[14-15]. Numerous studies have expounded that EpCAM can be used for CTC recognition when it is strongly expressed in tumors, yet it isn't useful in EpCAM-negative or low-expression tumors, such as melanoma[16-18]. Accordingly, such EpCAM-triggered CTCs detection leads to an inferior accuracy and sensitivity for melanoma in liquid biopsy. On the other hand, the sensitivity also involves with the brightness of the used luminescent probes in CTCs detection strategy. Since the commercial products of liquid biopsy are essentially based on the luminescence technique, photoluminescence quantum yields (PLQYs) of probes are crucial[5]. Nevertheless, the PLQYs of fluorescent dyes employed as commercial probes are still dissatisfactory (Fig. 2(h)); meanwhile, these products not only require the specific storage conditions, but also cannot be preserved for a long time based on factors such as activity, further affecting the accuracy and sensitivity[19-21].

To address these issues, we construct a new strategy of CTCs detection for liquid biopsy of melanoma by employing high-PLQYs metal halide perovskite(MHP) quantum dots(QDs) and strongly targeted-enrichment exosome as signal indicators and recognition analytes, respectively. Exosomes are vesicles surrounded by plasma membrane and released by cells into microenvironment; tumor-derived exosomes are derived from tumor cells and have a phospholipid configuration that promotes intercellular communication[22-23]. As a result, tumor-derived exosomes have a certain ability to target parent tumor cells, that is, "homing" properties, and to deliver exosome-encapsulated analytes to tumor sites[24-26]. Furthermore, MHP QDs as the emerging star optical materials have already shown great potential in optoelectronic applications due to their higher PLQY than fluorescent dyes. Becoming a superior photoluminescence (PL) indicator compared to conventional fluorescent dyes in biosensing, MHP QDs exhibit enhanced sensitivity and improved temporal-spatial resolution[27-29]. Recent developments of MHP QDs also further push the envelope on fighting hygroscopicity, toxicity, photo and thermal instability, thus activating a gratifying anticipation as optical probe of liquid biopsy[30-35].

2 Experiment

2.1 Materials

Cesium bromide (CsBr, Macklin, 99.999%), lead bromide($PbBr_2$, Macklin, 99.999%), Oleic acid(OA, Aladdin, 90%), Oleylamine(OAm, Aladdin, 99%), N, N-Dimethylformamide (DMF, Aladdin, 99.5%), Tetramethoxysilane(TMOS, Energy Chemical, 99%), Toluene(DAMAO, 99.95%) were used

directly without further purification. Phosphoethanolamine-N-[methoxy(polyethylene glycol)-2000], (mPEG-DSPE, MW 2 000 u) was bought from Tanshtech. For cell culture, phosphate buffer(PBS), dulbecco's modified eagle medium(DMEM), penicillin streptomycin and fetal bovine serum (FBS) were bought from Gibco. The B16 cell lines were purchased from Sigma-Aldrich(ECACC, 93021013 and 85111505). Antibody against TSG101(ab125011) was purchased from Abcam.

2.2 Synthesis of $CsPbBr_3@SiO_2$

$CsPbBr_3@SiO_2$ were prepared *via* one-pot route. 0.147 2 g $PbBr_2$, 0.086 8 g CsBr, 0.6 mL OAm and 1.8 mL OA were added into 10 mL DMF. Then the mixture was stirred at 60 ℃ for 1 h to obtain a clear solution. Ammonia solution (40 μL, 2.8%) was added into 2 mL of the precursor solution. After this, 0.2 mL of the precursor solution was rapidly added to 10 mL of dry toluene containing 5 μL of TMOS under vigorous agitation(1 500 r/min). After 10 s, the shaking rate was set to 150 r/min and maintained for 120 min. The final products were collected by centrifuging to 10 000 r/min for 5 min and dried at 60 ℃.

2.3 Fabrication of $CsPbBr_3@SiO_2@PEG$

The obtained powders were disposed simply by ultrasonic, thus being uniformly dispersed in water. Then mPEG-DSPE was adder into the solution and treated with ultrasound for several minutes. The products were collected by centrifugation and washed for several times with water to remove the residual reactants.

2.4 Isolation and Protein Analysis of Exosomes

In brief, exosomes were isolated by classical differential ultracentrifugation[36]. The cells were discarded from the collected B16 cells culture medium by centrifugation at a low speed of 500 × *g*, the supernatant was collected and further centrifugated at a speed of 16 500 × *g*. Then the cell debris and bullae were removed from the collected supernatant by filtration through a 0.22 μm sterile filter. After final 110 000 × *g* centrifugation, concentrated exosomes were collected, washed with PBS once, and then stored at 4 ℃. The protein components of purified exosomes were determined by BCA protein concentration kit followed the instructions. The surface marker of exosomes was identified by western blot, Anti-TSG101 was used as primary antibodies.

2.5 Preparation of PSPE

The above obtained nanomaterials were mixed with a certain amount of MEX, then the mixture was extruded through a polyester porous membrane in a micro extruder for 15 times. After extruding, the mixture was centrifuged at 10 000 r/min for 5 min and the supernatant was removed. The precipitate was then redispersed in PBS and washed three times with PBS. The obtained product was stored at 4 ℃.

2.6 Cell Culture

B16 cells were routinely cultured in DMEM medium with 10% FBS, and 1% penicillin/streptomycin (10 000 U/mL) in an incubator(5% CO_2, 37 ℃). Once cells reached 80% confluency, they were trypsinized(Trypsin, Thermo Fisher Scientific) and the cell suspension was used for the experiment.

2.7 *In Vitro* Cytotoxicity Assay

$CsPbBr_3$ QDs, $CsPbBr_3@SiO_2$, and $CsPbBr_3@SiO_2@PEG$ were dispersed in fresh culture medium for following experiment. Then B16 cells were seeded in a 96-well plate at a density of 1×10^4 cells per well overnight and then incubated with the pre-prepared reagent at different concentrations for 24 hours. Subsequently, the cells were treated with 100 μL of 3-(4,5-dimethyl-2-thiazolyl)-2,5-diphenyl-2-H-tetrazoliu bromide(MTT) reagent for 2 h. Before detection, 150 μL DMSO was added into each well and the absorbance at 490 nm was measured using a microplate reader.

2.8 Cellular Uptake of PSPE

In this study, B16 cells were used as the target cells. The B16 cell suspension was loaded into a cell culture dish (1×10^4) and then incubated at 37 ℃ for 24 h. PSPE was introduced into the culture medium(without FBS) of B16 cells and co-cultured for 30 min. Subsequently, the culture medium was removed, the cells were fixed with 4% paraformaldehyde for 15 minutes. After fixing, the cells were washed three times with PBS. Lastly, the cells were imaged *via* a Zeiss laser confocal microscope

(LSM980).

2.9 Targeting Efficiency of PSPE

The B16 cells(1×10^6 cells) incubated with PSPE (0.25 μg/mL) for different durations with gentle shaking at 37 ℃. After incubation, the sample underwent centrifugation at 1 500 r/min for 3 min. Next, the supernatant was discarded, and the sample was washed three times with PBS. Finally, the number of labeled cells was analyzed using flow cytometry.

2.10 Measurement and Characterization

Transmission electron microscopy (TEM) images and elemental mapping were acquired by an FEI Talos F200S microscope. XRD data were measured by a Bruker D8 Advance, Cu Kα radiation (λ = 0.154 06 nm), and the operating voltage and current were measured at 50 kV and 40 mA, respectively. The Fourier transform infrared (FTIR) were taken using a Thermo Scientific Nicolet IS50 FTIR spectrometer. The PL spectrum was measured by the Fluorolog-3 fluorescence spectrometer (HORIBA Instruments Incorporated). Confocal laser scanning microscope (CLSM, Zeiss, LSM980) was employed for cell imaging.

3 Results and Discussion

As shown in Fig. 1, we first synthesized $CsPbBr_3@SiO_2$ *via* one-pot route with some modifications[37-38]. Then, amorphous silicon was coated onto the surface of $CsPbBr_3$ QDs, forming $CsPbBr_3@SiO_2$ nanoparticles (NPs) with core-shell structure. Subsequently, to further improve the hydrophilicity and dispersibility of $CsPbBr_3@SiO_2$, the obtained NPs were loaded into the micelles constituted by PEG-grafted phospholipid (mPEG-DSPE) and formed $CsPbBr_3@SiO_2@PEG$. Finally, the exosomes derived from melanoma cells were selected to endow $CsPbBr_3@SiO_2@PEG$ with ability to target melanoma cells because of their "homing" ability. The as-prepared $CsPbBr_3@SiO_2@PEG$ and melanoma-derived exosome (MEX) were encapsulated together to form $CsPbBr_3@SiO_2@PEG@EV$ (PSPE) by being squeezed through a filter membrane physically in an extruder. In a word, exosome-triggered MHP-mediated CTCs detection would show enormous potential in

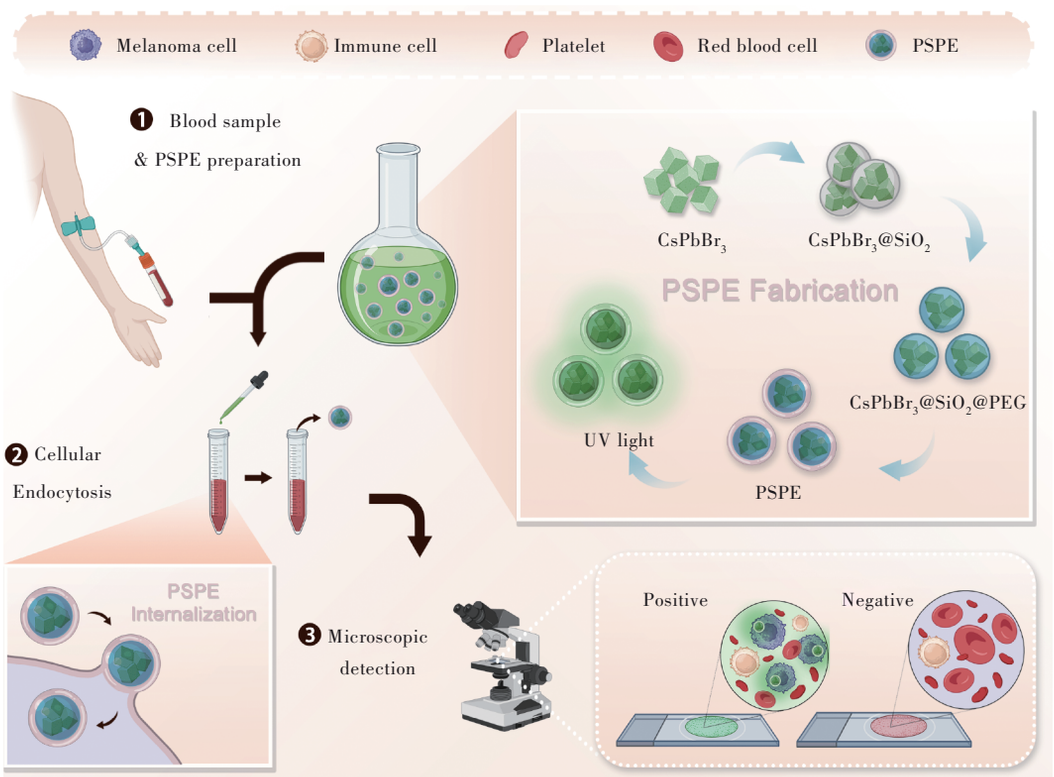

Fig.1 A schematic description of the production of exosome-triggered metal halide perovskite-mediated for melanoma CTCs detection

accurate melanoma CTCs diagnosis of liquid biopsy.

$CsPbBr_3$ QDs were synthesized through a one-step method at room temperature. $CsPbBr_3$ QDs exhibited a cubic shape with a mean length of 20 nm in the TEM images(Fig. 2(a)), and the corresponding elemental mapping images demonstrated a uniform distribution of Cs, Pb, and Br elements.

In the TEM images of $CsPbBr_3@SiO_2$(Fig. 2(b)), $CsPbBr_3@SiO_2$ NPs were all monodispersed nanospheres. The distribution of the Si element further confirmed the successfully coating of SiO_2 on the surface of $CsPbBr_3$ QDs. Fig. 2(c) presented a larger view of $CsPbBr_3@SiO_2$, which exhibited a mean diameter of 60 nm. X-ray diffraction (XRD) patterns

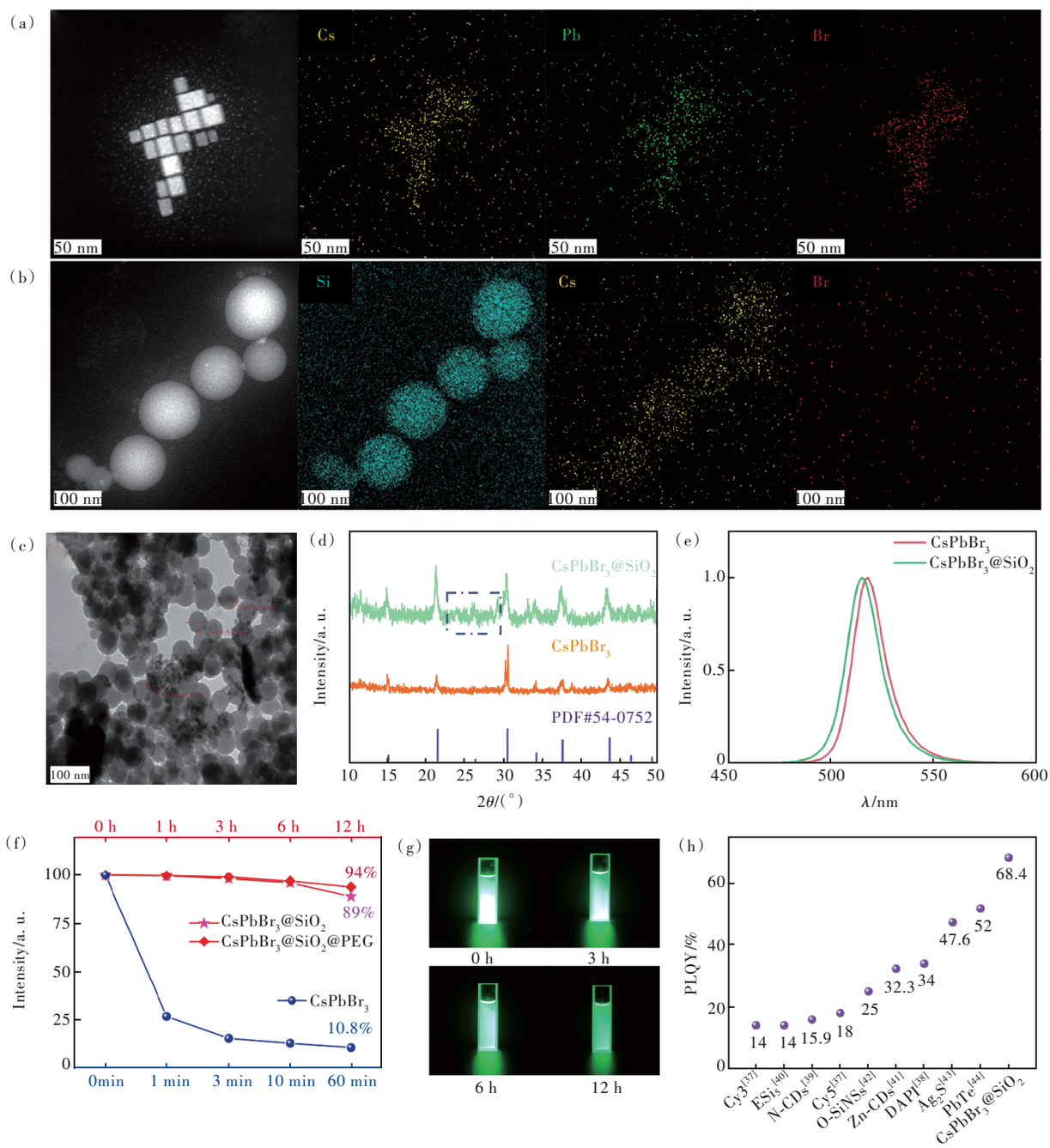

Fig.2　TEM images and corresponding elemental mapping images of $CsPbBr_3$ QDs(a) and $CsPbBr_3@SiO_2$(b). (c) TEM image of $CsPbBr_3@SiO_2$. (d) XRD patterns of $CsPbBr_3$ QDs and $CsPbBr_3@SiO_2$. (e) Emission spectra of $CsPbBr_3$ QDs and $CsPbBr_3@SiO_2$. (f) Time-dependent PL intensity variation of $CsPbBr_3$, $CsPbBr_3@SiO_2$, $CsPbBr_3@SiO_2$@PEG in aqueous solution. (g) Optical photograph of $CsPbBr_3@SiO_2$ under 365 nm UV light irradiation. (h) PLQYs comparison of different fluorescent materials[41-48]

were utilized to confirm the formations of $CsPbBr_3$ QDs and $CsPbBr_3@SiO_2$. In Fig. 2(d), XRD diffraction peaks of $CsPbBr_3$ QDs matched well with the standard card (PDF No. 54-0752). Additionally, a small and broad shoulder diffraction peak was observed at $2\theta = 26.2^\circ$, indicating the presence of low crystallinity amorphous silicon on the surface of $CsPbBr_3@SiO_2$[33,39-40].

Fig. 2(e) showed the PL spectra of $CsPbBr_3$ QDs and $CsPbBr_3@SiO_2$. The PL spectrum of $CsPbBr_3@SiO_2$ exhibited a slight shift compared to that of $CsPbBr_3$ QDs, which was attributed to the restriction imposed by the SiO_2 shell[37]. Moreover, the SiO_2 shell greatly enhanced the stability of $CsPbBr_3@SiO_2$. As shown in Fig. 2(f), the PL intensity of $CsPbBr_3$ QDs in water decreased to 26.6% within 1 min and to 10.8% within 60 min. However, $CsPbBr_3@SiO_2$ exhibited excellent dispersity and retained stable green luminescence for 12 h (Fig. 2(g)), indicating the SiO_2 shell effectively enhances the stability of $CsPbBr_3@SiO_2$. The PL intensity of $CsPbBr_3@SiO_2$ remained at 89% even after 12 h of dispersion in water, as depicted in Fig. 2(f), demonstrating excellent stability. Additionally, the confinement of the $CsPbBr_3$ core and the presence of the SiO_2 shell might synergistically enhance the photoluminescence quantum yield (PLQY) of $CsPbBr_3@SiO_2$ to 68.4% (Fig. 2(h)).

Here, $CsPbBr_3@SiO_2$ NPs are anticipated to serve as luminescent probes for liquid biopsy. The cytotoxicity tests were performed on B16 mouse melanoma cells using the MTT assay. Fig. 3(a) and (b) show that the cell viabilities of B16 cells decreased to below 70% after a 24-h incubation with $CsPbBr_3$ QDs and $CsPbBr_3@SiO_2$. To mitigate the cytotoxicity, $CsPbBr_3@SiO_2$ was encapsulated with mPEG-DSPE, a compound comprising a hydrophilic head and a hydrophobic tail, through self-assembly[49]. After being mixed with mPEG-DSPE and subjected to ultrasound for several minutes, $CsPbBr_3@SiO_2@PEG$ composites were formed. Fig. 3(c) demonstrates the improved viability of B16 cells, attributed to the protection provided by mPEG-DSPE. The results reveal that the viabilities of B16 cells reached nearly 100% after co-incubation with $CsPbBr_3@SiO_2@PEG$ for 24 h, with a corresponding concentration increase from 0.15 mg/mL to 1.25 mg/mL. Thus, $CsPbBr_3@SiO_2@PEG$ demonstrated excellent biocompatibility. Furthermore, the encapsulation of mPEG-DSPE does not affect the stability of $CsPbBr_3@SiO_2@PEG$ (Fig. 2(f)).

The scanning electron microscope (SEM) and TEM were utilized to characterize the morphology of $CsPbBr_3@SiO_2@PEG$ NPs. Fig. 3(d) and (e) display the monodisperse spheric morphology of $CsPbBr_3@SiO_2@PEG$ NPs. The elemental mapping revealed the distribution of N and P elements, which originates from mPEG-DSPE, confirming the successful coating of mPEG-DSPE on the surface of $CsPbBr_3@SiO_2$. The above results were further confirmed by the FTIR spectra.

The FTIR results were consistent with the above results. As depicted in Fig. 3(f), the characteristic peak at 1 095 cm^{-1} was attributed to the Si—O—Si vibration of the amorphous SiO_2, which results from the formation of more cross-linked SiO_2 networks through the hydrolysis process of TMOS[50]. A strong ridge was observed at 2 925 cm^{-1}, which was attributed to —CH_2CH_2O— in the PEG portion of mPEG-DSPE[51]. The successful encapsulation of $CsPbBr_3@SiO_2@PEG$ was further confirmed by XRD patterns. In Fig. 3(g), the characteristic diffraction peaks at 11.9°, 18.9° and 23.1° were attributed to the mPEG-DSPE, demonstrating the existence of mPEG-DSPE on the surface of $CsPbBr_3@SiO_2@PEG$. Subsequently, the hydrodynamic size of the $CsPbBr_3@SiO_2@PEG$ in PBS was evaluated *via* the dynamic light scattering (DLS) technique. As indicated in Fig. 3(h), the $CsPbBr_3@SiO_2@PEG$ exhibited an average diameter of ~70 nm.

As known to us, tumor-derived exosomes have attracted more and more attention due to their unique features such as minimal immunogenicity and toxicity, efficient cargo loading, preferred tumor homing, *etc*[52-56]. In order to endow the potential application of $CsPbBr_3@SiO_2@PEG$ for liquid biopsy, melanoma-derived exosome (MEX) was selected as recognition analyte for its unique biological characteristics.

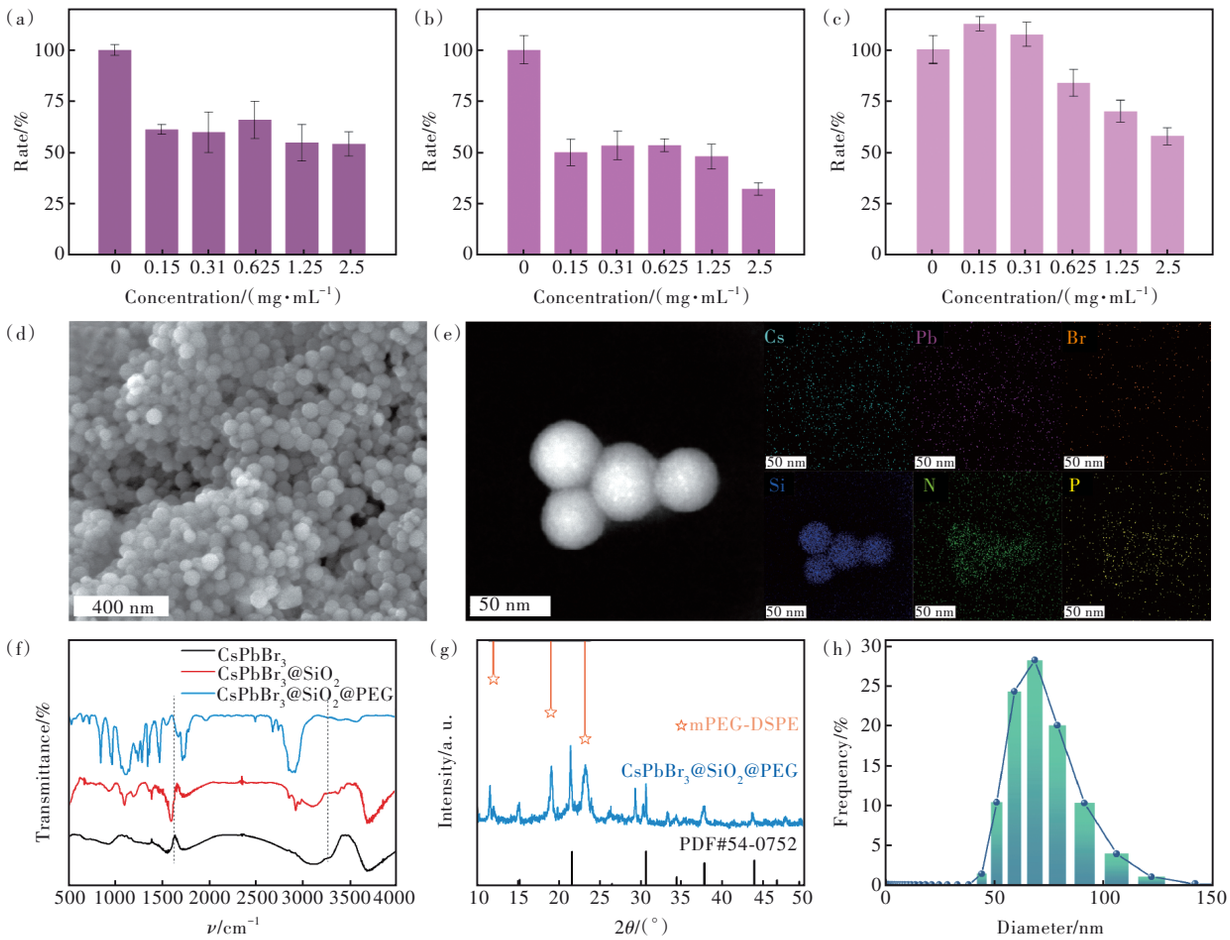

Fig. 3　Cytotoxicity analyses of $CsPbBr_3$ QDs(a), $CsPbBr_3$@SiO_2(b), and $CsPbBr_3$@SiO_2@PEG(c). (**R7**) SEM(d) and TEM (e) and corresponding elemental mapping images of $CsPbBr_3$@SiO_2@PEG. (f) FTIR spectra of $CsPbBr_3$ QDs, $CsPbBr_3$@SiO_2 and $CsPbBr_3$@SiO_2@PEG. (g) XRD pattern of $CsPbBr_3$@SiO_2@PEG. (h) Hydrodynamic diameter distribution of $CsPbBr_3$@SiO_2@PEG

As shown in Fig. 4(a), MEX was extracted from the collected culture medium of B16 cells *via* classical differential ultracentrifugation[57]. Then, the obtained exosomes were used to load $CsPbBr_3$@SiO_2@PEG and form melanoma cells targeted nanoprobes PSPE by the physical extrusion method[58].

Micromorphology analysis *via* TEM was performed on MEX. In Fig. 4(b), a typical exosome structure was observed with a diameter of ~50 nm. The successful extraction of MEX was confirmed by the detection of exosomal-specific protein TSG101 through western blot experiments, as illustrated in Fig. 4(d)[59]. The as-prepared MEX was blended with $CsPbBr_3$@SiO_2@PEG and subsequently extruded to generate exosome membrane-cloaked PSPE. After extruding, the exosome layer can be observed in the TEM image of PSPE(Fig. 4(c)). Furthermore, as shown in Fig. 4(d), TSG101 was found in PSPE *via* western blotting, illustrating the successful coating of MEX on the surface of PSPE. Zeta potential change from −3.63 mV to −9.62 mV in the PSPE after modification with MEX(Fig. 4(e)) and the presence of characteristic protein absorption peaks around 1 634 cm^{-1}(C═O)(Fig. 4(f)) further confirmed the extrusion self-assembly method[60]. In addition, the hydrodynamic diameter of the PSPE increased to ~240 nm(Fig. 4(g)). Notably, compared to $CsPbBr_3$@SiO_2@PEG, PSPE exhibited a slight blue shift in its PL emission peak at 504 nm.

Although all cells exhibit nonspecific uptake, which affects the specificity and sensitivity of detection, tumor-derived exosomes can specifically target parental tumor cells without further modification[54, 61]. The proteins and complex lipids on the surface of

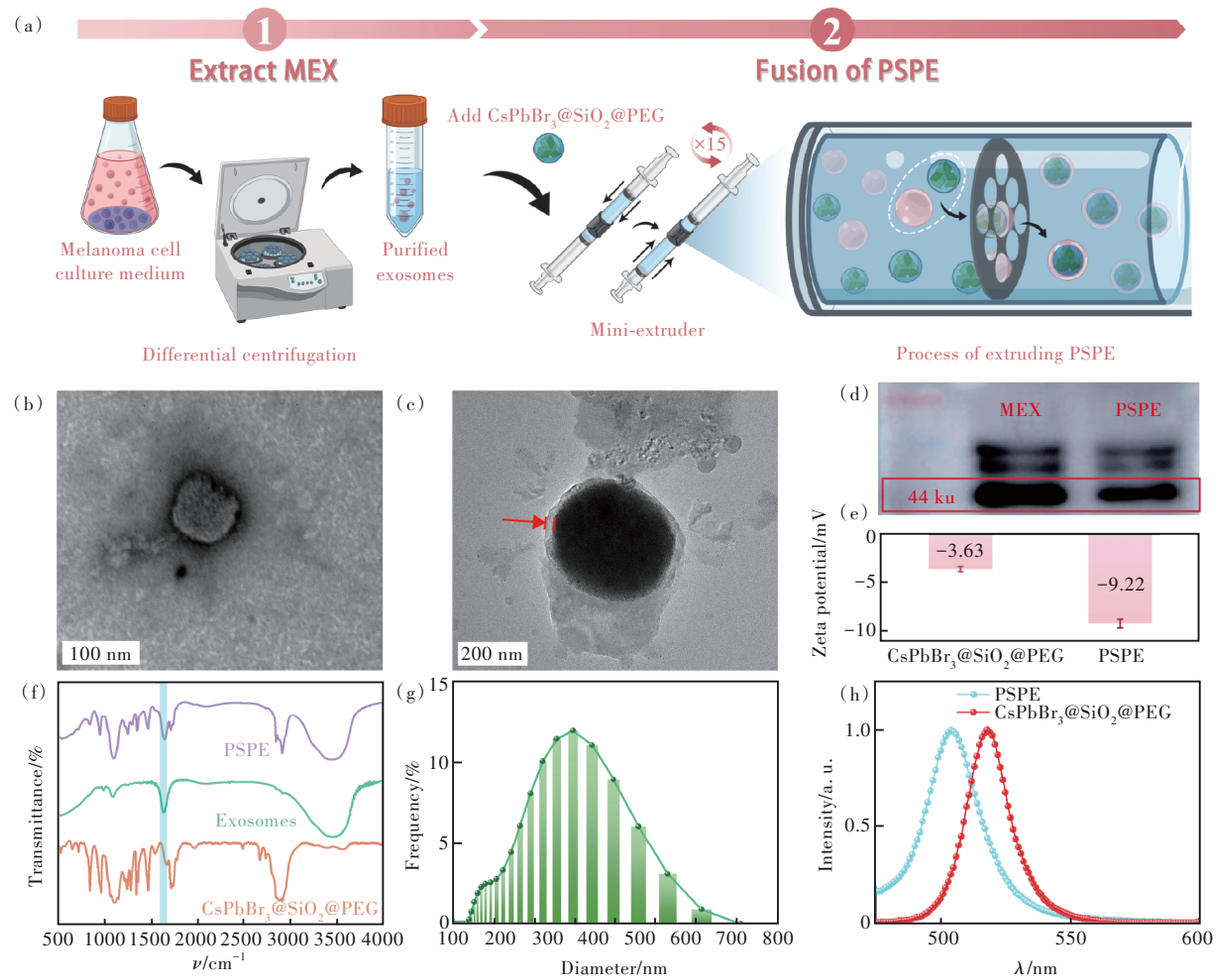

Fig.4 (a) Schematic diagrams of the extracting process of MEX and the extrusion process of PSPE. TEM images of MEX (b) and PSPE (c). (d) Western blot image of MEX and PSPE. Zeta potential analysis (e), and FTIR spectra (f) of $CsPbBr_3$@SiO_2@PEG and PSPE. (g) Hydrodynamic diameter distribution of PSPE. (h) PL spectrum of $CsPbBr_3$@SiO_2@PEG and PSPE

tumor-derived exosomes, as well as the conservation of tropism between parent and recipient cells contribute to the targeting ability of exosomes[62-64].

To verify the capability of PSPE as a fluorescent probe, we introduced PSPE into the culture medium of melanoma B16 cells and co-cultured them. Then, as shown in Fig. 5(a), we conducted CLSM *z*-stack scanning from the *z*-axis range of 0 to 35 μm, with 5 μm-step intervals, to verify the PSPE incorporation within the cells. The merged images of bright-field images and PSPE fluorescence in dark-field images taken at different depths *via* *z*-stack scanning were presented in Fig. 5(b). Although cell morphology is visible throughout the range of z = 5−30 μm, the fluorescence of PSPE is observable in the range of z = 10−25 μm. Subsequently, we constructed a three-dimensional model of PSPE fluorescence from the dark-field images. The stereoscopic fluorescence model in Fig. 5(c) confirms the uptake of PSPE by the B16 cells. These results suggest that PSPE nanoprobes were internalized within the cells and can be utilized as effective nanoprobes for detecting melanoma cells.

Flow cytometry was utilized to evaluate the efficiency of PSPE in labeling B16 cells. Fig. 5(d) displays the low targeting efficiency of the commercialized Anti-EpCAM antibody in targeting B16 cells. However, after being co-cultured with PSPE for different durations, the efficiency of labeling reached its peak at 40 min before reaching a plateau. In contrast to commercial Anti-EpCAM antibody, the detection sensitivity of our reagent materials was raised

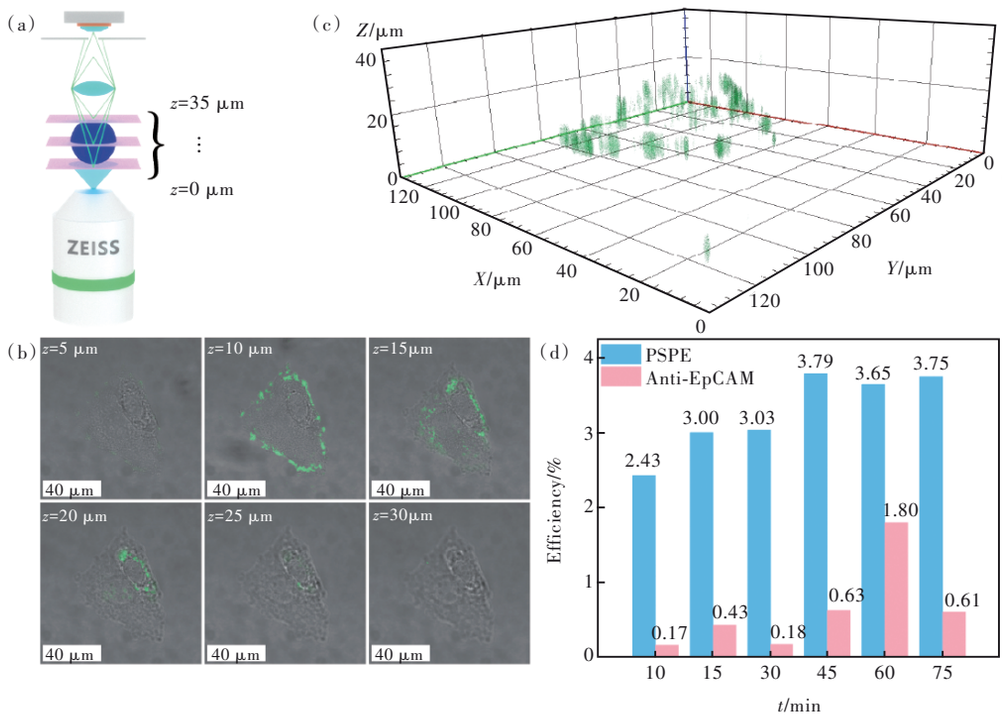

Fig.5　(a) Schematic diagrams of confocal laser scanning microscope *z*-stack scanning setup. (b) Merged fluorescence with bright-field images from *z*-stack scanning at the same region. The images are taken with a 5 μm-step. (c) Three-dimensional model image of PSPE fluorescence based on the z-stack images. (d) Flow cytometry evaluating the efficiency of PSPE labeling melanoma cells

up by an order of magnitude. It indicated that exosomes could promote nanomaterials to target parent tumor cells. For melanoma cells, the labeling efficiency of PSPE was almost ten-fold higher than that of the Anti-EpCAM antibodies, demonstrating that MEX exhibited considerable potential in detecting melanoma CTCs and could significantly improve the internalization of CTCs.

4　Conclusion

We have developed a new nanoscale probe for detecting CTCs in melanoma. This nanoprobe is composed of high PLQY perovskite quantum dots as signal generators and melanoma-derived exosomes as biosensing elements. Due to their poor stability, pure $CsPbBr_3$ QDs are difficult to apply in the field of biomedicine. By encapsulating them with SiO_2 and mPEG-DSPE, we significantly improved their stability, PLQY, and biological compatibility, eventually leading to the successful development of $CsPbBr_3$@SiO_2@PEG. After loading with melanoma-derived exosomes that possess the homing ability, $CsPbBr_3$@SiO_2@PEG is endowed with biological targeting capability, forming PSPE nanoprobe. Finally, we performed proof-of-concept experiments to show the cellular uptake and the melanoma cells labeling. The results suggest that the PSPE nanoprobe may find applications in detecting melanoma CTCs.

Response Letter is available for this paper at: http://cjl.lightpublishing.cn/thesisDetails#10.37188/CJL.20230237.

References:

[1] LUKE J J, FLAHERTY K T, RIBAS A, *et al.* Targeted agents and immunotherapies: optimizing outcomes in melanoma [J]. *Nat. Rev. Clin. Oncol.*, 2017, 14(8): 463-482.

[2] RODRÍGUEZ-CERDEIRA C, CARNERO GREGORIO M, LÓPEZ-BARCENAS A, *et al.* Advances in immunotherapy for melanoma: a comprehensive review [J]. *Mediators Inflamm.*, 2017, 2017: 3264217.

[3] DE RUBIS G, RAJEEV KRISHNAN S, BEBAWY M. Liquid biopsies in cancer diagnosis, monitoring, and prognosis [J]. *Trends Pharmacol. Sci.*, 2019, 40(3): 172-186.

[4] ZHE X N, CHER M L, BONFIL R D. Circulating tumor cells: finding the needle in the haystack [J]. *Am. J. Cancer Res.*, 2011, 1(6): 740-751.

[5] DING P, WANG Z L, WU Z E, *et al*. Natural biointerface based on cancer cell membranes for specific capture and release of circulating tumor cells [J]. *ACS Appl. Mater. Interfaces*, 2020, 12(18): 20263-20270.

[6] HAI P F, QU Y, LI Y, *et al*. Label-free high-throughput photoacoustic tomography of suspected circulating melanoma tumor cells in patients *in vivo* [J]. *J. Biomed. Opt.*, 2020, 25(3): 1-17.

[7] LIM S H, BECKER T M, CHUA W, *et al*. Circulating tumour cells and circulating free nucleic acid as prognostic and predictive biomarkers in colorectal cancer [J]. *Cancer Lett.*, 2014, 346(1): 24-33.

[8] ZHANG H K, YUAN F N, QI Y Z, *et al*. Circulating tumor cells for glioma [J]. *Front. Oncol.*, 2021, 11: 607150.

[9] MA C H, ZHANG L J, HU H X, *et al*. Clinical application of circulating tumor cell detection: the challenges and solutions [J]. *Chin. J. Pathol.*, 2022, 51(3): 276-280. (in Chinese)

[10] VEDOVA P D, ILIEVA M, ZHURBENKO V, *et al*. Gold nanoparticle-based sensors activated by external radio frequency fields [J]. *Small*, 2015, 11(2): 248-256.

[11] WANG L W, PENG C W, CHEN C, *et al*. Quantum dots-based tissue and in vivo imaging in breast cancer researches: current status and future perspectives [J]. *Breast Cancer Res. Treat.*, 2015, 151(1): 7-17.

[12] KIM J H, CHUNG H H, JEONG M S, *et al*. One-step detection of circulating tumor cells in ovarian cancer using enhanced fluorescent silica nanoparticles [J]. *Int. J. Nanomed.*, 2013, 8: 2247-2257.

[13] ZHANG J, SHIKHA S, MEI Q S, *et al*. Fluorescent microbeads for point-of-care testing: a review [J]. *Microchim. Acta*, 2019, 186(6): 361.

[14] GAO Y, GU S E, ZHANG Y Y, *et al*. The architecture and function of monoclonal antibody-functionalized mesoporous silica nanoparticles loaded with mifepristone: repurposing abortifacient for cancer metastatic chemoprevention [J]. *Small*, 2016, 12(19): 2595-2608.

[15] VAN DER GUN B T F, MELCHERS L J, RUITERS M H J, *et al*. EpCAM in carcinogenesis: the good, the bad or the ugly [J]. *Carcinogenesis*, 2010, 31(11): 1913-1921.

[16] LIN D F, SHEN L S, LUO M, *et al*. Circulating tumor cells: biology and clinical significance [J]. *Signal Transduct. Target. Ther.*, 2021, 6(1): 404.

[17] GAISER M R, VON BUBNOFF N, GEBHARDT C, *et al*. Liquid biopsy to monitor melanoma patients [J]. *J. Dtsch. Dermatol. Ges.*, 2018, 16(4): 405-414.

[18] RAPANOTTI M C, CAMPIONE E, SPALLONE G, *et al*. Minimal residual disease in melanoma: circulating melanoma cells and predictive role of MCAM/MUC18/MelCAM/CD146 [J]. *Cell Death Discov.*, 2017, 3(1): 17005.

[19] DENG H, YU H T. Silver nanoparticle surface enabled self-assembly of organic dye molecules [J]. *Materials* (*Basel*), 2019, 12(16): 2592.

[20] GREEN A P, BUCKLEY A R. Solid state concentration quenching of organic fluorophores in PMMA [J]. *Phys. Chem. Chem. Phys.*, 2015, 17(2): 1435-1440.

[21] CHELONI G, SLAVEYKOVA V I. Optimization of the C11-BODIPY$^{581/591}$ dye for the determination of lipid oxidation in *Chlamydomonas reinhardtii* by flow cytometry [J]. *Cytometry* A, 2013, 83(10): 952-961.

[22] THAKUR A, PARRA D C, MOTALLEBNEJAD P, *et al*. Exosomes: small vesicles with big roles in cancer, vaccine development, and therapeutics [J]. *Bioact. Mater.*, 2021, 10: 281-294.

[23] SRIVASTAVA A, RATHORE S, MUNSHI A, *et al*. Organically derived exosomes as carriers of anticancer drugs and imaging agents for cancer treatment [J]. *Semin. Cancer Biol.*, 2022, 86: 80-100.

[24] QIAO L, HU S Q, HUANG K, *et al*. Tumor cell-derived exosomes home to their cells of origin and can be used as trojan horses to deliver cancer drugs [J]. *Theranostics*, 2020, 10(8): 3474-3487.

[25] DESGROSELLIER J S, CHERESH D A. Integrins in cancer: biological implications and therapeutic opportunities [J]. *Nat. Rev. Cancer*, 2010, 10(1): 9-22.

[26] JAISWAL S, JAMIESON C H M, PANG W W, *et al*. CD47 is upregulated on circulating hematopoietic stem cells and leukemia cells to avoid phagocytosis [J]. *Cell*, 2009, 138(2): 271-285.

[27] LIGNOS I, STAVRAKIS S, NEDELCU G, *et al*. Synthesis of cesium lead halide perovskite nanocrystals in a droplet-

based microfluidic platform: fast parametric space mapping [J]. *Nano Lett.*, 2016, 16(3): 1869-1877.

[28] WANG G, YU S J, LIU B, *et al.* Nanocomposites of $CsPbBr_3$ perovskite quantum dots embedded in Gd_2O_3:Eu^{3+} hollow spheres for LEDs application [J]. *J. Rare Earths*, 2022, 40(10): 1509-1518.

[29] SHAH S A A, SAYYAD M H, SUN J H, *et al.* Recent advances and emerging trends of rare-earth-ion doped spectral conversion nanomaterials in perovskite solar cells [J]. *J. Rare Earths*, 2022, 40(11): 1651-1667.

[30] XU X M, PAN Y L, GE L, *et al.* High-performance perovskite composite electrocatalysts enabled by controllable interface engineering [J]. *Small*, 2021, 17(29): 2101573.

[31] MA X J, YANG W, GE X, *et al.* Design a novel multifunctional($CsPbBr_3$/Fe_3O_4)@MPSs@SiO_2 magneto-optical microspheres for capturing circulating tumor cells [J]. *Appl. Surf. Sci.*, 2021, 551: 149427.

[32] ZHAO Y, LI C L, JIANG J Z, *et al.* Sensitive and stable tin-lead hybrid perovskite photodetectors enabled by double-sided surface passivation for infrared upconversion detection [J]. *Small*, 2020, 16(26): 2001534.

[33] YAN Q B, BAO N, DING S N. Thermally stable and hydrophilic $CsPbBr_3$/mPEG-NH_2 nanocrystals with enhanced aqueous fluorescence for cell imaging [J]. *J. Mater. Chem.* B, 2019, 7(26): 4153-4160.

[34] 丁梦宇, 郑标, 魏维平, 等. 单分散$CsPbBr_3$@SiO_2纳米颗粒制备及其在柔性显示与荧光防伪中的应用 [J]. 发光学报, 2022, 43(8): 1309-1318.
DING M Y, ZHENG B, WEI W P, *et al.* Synthesis of monodisperse $CsPbBr_3$@SiO_2 nanoparticles for flexible display and anti-counterfeiting [J]. *Chin. J. Lumin.*, 2022, 43(8): 1309-1318. (in Chinese)

[35] 王栋, 兰月梅, 刘劝, 等. 白光LED用$CsPbBr_3$钙钛矿量子点玻璃制备及其稳定性 [J]. 发光学报, 2021, 42(12): 1863-1871.
WANG D, LAN Y M, LIU Q, *et al.* Preparation and stability of $CsPbBr_3$ perovskite quantum dots glass for white LED [J]. *Chin. J. Lumin.*, 2021, 42(12): 1863-1871. (in Chinese)

[36] YANG D B, ZHANG W H, ZHANG H Y, *et al.* Progress, opportunity, and perspective on exosome isolation-efforts for efficient exosome-based theranostics [J]. *Theranostics*, 2020, 10(8): 3684-3707.

[37] ZHONG Q X, CAO M H, HU H C, *et al.* One-pot synthesis of highly stable $CsPbBr_3$@SiO_2 core-shell nanoparticles [J]. *ACS Nano*, 2018, 12(8): 8579-8587.

[38] KUMAR P, PATEL M, PARK C, *et al.* Highly luminescent biocompatible $CsPbBr_3$@SiO_2 core-shell nanoprobes for bioimaging and drug delivery [J]. *J. Mater. Chem.* B, 2020, 8(45): 10337-10345.

[39] PRAMANIK A, GATES K, PATIBANDLA S, *et al.* Water-soluble and bright luminescent cesium-lead-bromide perovskite quantum dot-polymer composites for tumor-derived exosome imaging [J]. *ACS Appl. Bio Mater.*, 2019, 2(12): 5872-5879.

[40] XU L M, CHEN J W, SONG J Z, *et al.* Double-protected all-inorganic perovskite nanocrystals by crystalline matrix and silica for triple-modal anti-counterfeiting codes [J]. *ACS Appl. Mater. Interfaces*, 2017, 9(31): 26556-26564.

[41] WAGGONER A. Covalent labeling of proteins and nucleic acids with fluorophores [J]. *Methods Enzymol*, 1995, 246: 362-373.

[42] LI J, DONG Y, WEI R W, *et al.* Stable, bright, and long-fluorescence-lifetime dyes for deep-near-infrared bioimaging [J]. *J. Am. Chem. Soc.*, 2022, 144(31): 14351-14362.

[43] CUI S T, WU Y F, LIU Y, *et al.* Synthesis of carbon dots with a tunable photoluminescence and their applications for the detection of acetone and hydrogen peroxide [J]. *Chin. Chem. Lett.*, 2020, 31(2): 487-493.

[44] HE Y, SU Y Y, YANG X B, *et al.* Photo and pH stable, highly-luminescent silicon nanospheres and their bioconjugates for immunofluorescent cell imaging [J]. *J. Am. Chem. Soc.*, 2009, 131(12): 4434-4438.

[45] XU Q, LIU Y, SU R G, *et al.* Highly fluorescent zn-doped carbon dots as fenton reaction-based bio-sensors: an integrative experimental-theoretical consideration [J]. *Nanoscale*, 2016, 8(41): 17919-17927.

[46] COSA G, FOCSANEANU K S, MCLEAN J R N, *et al.* Photophysical properties of fluorescent DNA-dyes bound to single- and double-stranded DNA in aqueous buffered solution [J]. *Photochem. Photobiol.*, 2001, 73(6): 585-599.

[47] PAN L J, TU J W, YANG L L, *et al.* Photoluminescence enhancement of NIR-II emissive Ag_2S quantum dots *via* chloride-mediated growth and passivation [J]. *Adv. Opt. Mater.*, 2022, 10(9): 2102806.

[48] MURPHY J E, BEARD M C, NORMAN A G, *et al.* PbTe colloidal nanocrystals: synthesis, characterization, and multiple exciton generation [J]. *J. Am. Chem. Soc.*, 2006, 128(10): 3241-3247.

[49] ZHAO C C, ZHANG X L, LI K B, *et al.* Forster resonance energy transfer switchable self-assembled micellar nano-

probe: ratiometric fluorescent trapping of endogenous H_2S generation *via* fluvastatin-stimulated upregulation [J]. *J. Am. Chem. Soc.*, 2015, 137(26): 8490-8498.

[50] SUN C, ZHANG Y, RUAN C, *et al*. Efficient and stable white leds with silica-coated inorganic perovskite quantum dots [J]. *Adv. Mater.*, 2016, 28(45): 10088-10094.

[51] YANG Z Y, XU J K, ZONG S F, *et al*. Lead halide perovskite nanocrystals-phospholipid micelles and their biological applications: multiplex cellular imaging and *in vitro* tumor targeting [J]. *ACS Appl. Mater. Interfaces*, 2019, 11(51): 47671-47679.

[52] BATTAGLIA L, SCOMPARIN A, DIANZANI C, *et al*. Nanotechnology addressing cutaneous melanoma: the italian landscape [J]. *Pharmaceutics*, 2021, 13(10): 1617.

[53] MKHOBONGO B, CHANDRAN R, ABRAHAMSE H. The role of melanoma cell-derived exosomes (MTEX) and photodynamic therapy(PDT) within a tumor microenvironment [J]. *Int. J. Mol. Sci.*, 2021, 22(18): 9726.

[54] ALIA MOOSAVIAN S, HASHEMI M, ETEMAD L, *et al*. Melanoma-derived exosomes: versatile extracellular vesicles for diagnosis, metastasis, immune modulation, and treatment of melanoma [J]. *Int. Immunopharmacol.*, 2022, 113: 109320.

[55] PRETTI M A M, BERNARDES S S, CRUZ J G VDA, *et al*. Extracellular vesicle-mediated crosstalk between melanoma and the immune system: impact on tumor progression and therapy response [J]. *J. Leukoc. Biol.*, 2020, 108(4): 1101-1115.

[56] VAKHSHITEH F, ATYABI F, OSTAD S N. Mesenchymal stem cell exosomes: a two-edged sword in cancer therapy [J]. *Int. J. Nanomed.*, 2019, 14: 2847-2859.

[57] WITWER K W, BUZÁS E I, BEMIS L T, *et al*. Standardization of sample collection, isolation and analysis methods in extracellular vesicle research [J]. *J. Extracell. Vesicles*, 2013, 2(1): 20360.

[58] VAN DEUN J, ROUX Q, DEVILLE S, *et al*. Feasibility of mechanical extrusion to coat nanoparticles with extracellular vesicle membranes [J]. *Cells*, 2020, 9(8): 1797.

[59] MO J T, DA X B, LI Q X, *et al*. The study of exosomes-encapsulated mPEG-PLGA polymer drug-loaded particles for targeted therapy of liver cancer [J]. *J. Oncol.*, 2022, 2022: 4234116.

[60] CHENG G, LI W Q, HA L, *et al*. Self-assembly of extracellular vesicle-like metal-organic framework nanoparticles for protection and intracellular delivery of biofunctional proteins [J]. *J. Am. Chem. Soc.*, 2018, 140(23): 7282-7291.

[61] GURUNG S, PEROCHEAU D, TOURAMANIDOU L, *et al*. The exosome journey: from biogenesis to uptake and intracellular signalling [J]. *Cell Commun. Signal.*, 2021, 19(1): 47.

[62] BELHADJ Z, HE B, DENG H L, *et al*. A combined "eat me/don't eat me" strategy based on extracellular vesicles for anticancer nanomedicine [J]. *J. Extracell. Vesicles*, 2020, 9(1): 1806444.

[63] ESCREVENTE C, KELLER S, ALTEVOGT P, *et al*. Interaction and uptake of exosomes by ovarian cancer cells [J]. *BMC Cancer*, 2011, 11: 108.

[64] PAROLINI I, FEDERICI C, RAGGI C, *et al*. Microenvironmental pH is a key factor for exosome traffic in tumor cells [J]. *J. Biol. Chem.*, 2009, 284(49): 34211-34222.

陈志山(1993-),男,广东汕尾人,博士研究生,2020年于广州医科大学获得硕士学位,主要从事荧光纳米材料体外检测方面的研究。
E-mail: zhishan_chen@qq.com

李杨(1984-),男,山东淄博人,博士,教授,博士生导师,2014年于华南理工大学获得博士学位,主要从事无机固体发光材料缺陷调控,特别是长余辉材料的设计、机理及应用的研究。
E-mail: lychris@sina.com

徐朋飞(1996-),男,江苏宿迁人,硕士,2023年于广州医科大学获得硕士学位,主要从事荧光纳米材料体外检测方面的研究。
E-mail: 2432368710@qq.com